Inorganic Chemistry

ARTICLE

pubs.acs.org/IC

Hydrolysis of Uranyl(VI) in Acidic and Basic Aqueous Solutions Using a Noncomplexing Organic Base: A Multivariate Spectroscopic and Statistical Study

Fabienne Quilès,* Chinh Nguyen-Trung,† Cédric Carteret, and Bernard Humbert‡

Laboratoire de Chimie Physique et Microbiologie pour l'Environnement (LCPME), UMR 7564, CNRS, Nancy-Université, 405 rue de Vandoeuvre, F-54600 Villers-lès-Nancy, France

Supporting Information

ABSTRACT: In the field of actinide aqueous chemistry, this work aims to resolve some controversy about uranyl(VI) hydroxide species present in basic aqueous solutions. We revisit the Raman, IR, and UV−visible spectra with two new approaches. First, Raman, IR and UV data were recorded systematically from aqueous solutions with the noncomplexing electrolyte $(C_2H_5)_4NNO_3$ at 25 °C and 0.1 MPa ($[U_{total}]$ = 0.005−0.105 M) in H_2O and D_2O over a wide range of −log $mH(D)^+$ between 2.92 and 14.50. Second, vibrational spectra (IR and Raman) of basic solutions in H_2O and D_2O were analyzed using the Bayesian Positive Source Separation method to estimate pure spectra of individual species. In D_2O solutions, the new spectroscopic data showed the occurrence of the same species as those in H_2O. As observed for the wavenumber of the symmetric stretching mode, the wavenumber characteristic of the O═U═O antisymmetric stretching mode decreases as the number of $OH(D)^-$ ligands increases. These kinds of data, completed by (1) analysis of the signal widths, (2) persistence of the apparent exclusion rule between IR and Raman spectra of the uranyl species stretching modes, and (3) interpretation of the absorption UV−visible spectra, allow discussion of the chemistry, structures, and polynuclearity of uranyl(VI) species. In moderate basic solutions, the presence of two trimers is suggested. In highly basic solutions ($[OH^-] \approx 3$ M), the two monomers $UO_2(OH)_4^{2-}$ and $UO_2(OH)_5^{3-}$ are confirmed to be in good agreement with earlier EXAFS and NMR results. The occurrence of the $UO_2(OH)_6^{4-}$ monomer is also suggested from the more basic solutions investigated.

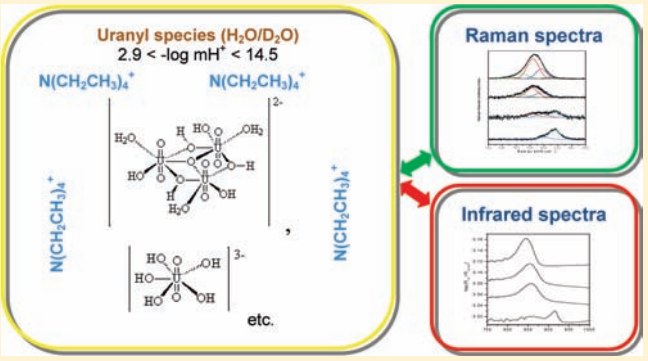

INTRODUCTION

Knowledge of the hydrolysis of the uranyl(VI) ion, particularly in highly basic solutions, is fundamental to a better understanding and modeling of actinide release from irradiated nuclear waste tanks surrounded by concrete and stored in deep underground vaults in contact with oxidizing natural water. The hydrolysis reactions of the hexavalent uranyl(VI) ion have been studied with various techniques.[1−13] In acidic solutions, $2 \leq -\log mH^+ \leq 5$,[14] experimental data obtained from potentiometric[4,15] and both Raman[2,10] and IR[10,16] vibrational spectroscopic measurements agree on the predominance of three species: UO_2^{2+}, $(UO_2)_2(OH)_2^{2+}$, and $(UO_2)_3(OH)_5^+$. In basic solutions, no consensus is available. Two series of species were claimed from potentiometric studies. Complexes $(UO_2)_3(OH)_7^-$, $(UO_2)_3(OH)_8^{2-}$, $(UO_2)_3(OH)_{10}^{4-}$, $(UO_2)_3(OH)_{11}^{5-}$, and $UO_2(OH)_4^{2-}$ have been suggested,[4] whereas complexes $(UO_2)_3(OH)_7^-$, $(UO_2)_4(OH)_7^-$, $UO_2(OH)_3^-$, and $UO_2(OH)_4^{2-}$ were proposed in other studies.[13,15] There is agreement that several mononuclear and polynuclear species coexist in basic solutions, but controversy remains concerning their structure. Only one study covered a wide −log mH^+ range to tentatively have information on the species at −log $mH^+ > 12$, by analysis of the Raman spectra.[9] However, a correct interpretation of the spectra was precluded because of the lack of data by other spectroscopic methods and because some Raman scattering bands of tetramethylammonium hydroxide used as a base overlapped the Raman scattering bands of uranyl. In highly basic solutions (−log $mH^+ > 13$), EXAFS and ^{17}O NMR measurements suggested the predominance of two monomers, $UO_2(OH)_4^{2-}$ and $UO_2(OH)_5^{3-}$.[5−7] Although a large number of experimental studies were devoted to the study of the hydrolysis of the uranyl(VI) ion, the data are incomplete and scattered. This is mainly because all of those studies have been developed at different experimental conditions, −log mH^+ ranges did not necessarily overlap, and supporting electrolytes, temperatures of analysis, and uranium concentrations were very different.[1,4−7,9,17] Moreover, there is a lack of data, particularly in the −log mH^+ range 12−14. One aim of this work was then to explore the −log mH^+ and −log mD^+ range between 11 and 14.5, which

Received: September 24, 2010
Published: February 28, 2011

overlap potentiometric titration domains and both EXAFS and NMR measurements.

Previous vibrational spectra showed a general tendency of decreasing values for the O═U═O stretching mode wavenumbers with increases in hydrolysis[2,4,9,10,18] or by coordination with ligands.[19−22] The uranyl(VI) group was shown to be linear in species UO_2^{2+} and $UO_2(OH)_4^{2-}$.[23,24] For each hydroxide complex, it was suggested that only one band is observed whatever its structure (dimer, trimer, etc.).[2,4,10] However, four vibrations can be expected on the basis of the U═O bonds for the dimer that belongs to the D_{2h} group (A_g and B_{2g} and also B_{1u} and B_{3u} modes would be Raman- and IR-active, respectively). However, even though some theoretical calculations suggested an O═U═O angle of 170° for the dimer,[25] only two bands were observed.[10] One has to verify whether features similar to those observed in acidic media could be observed in the vibrational spectra of species in basic solutions. Because D_2O does not absorb in the 1000−700 cm^{-1} region, better quality IR spectra in the attenuated total reflection mode (IR-ATR) can be expected in the region of the uranyl(VI) stretching mode. Structural data on the UO kind of coupling between uranium and oxygen atoms from OH^- and O^{2-} ligands and the arrangement around the uranium atom should be obtained. Indeed, deuteration of uranyl(VI) samples could drastically change the wavenumbers of the U═O stretching modes if ligands and D_2O are not in the equatorial plane, leading to possible mechanical coupling. Knowledge of the wavenumbers of both uranyl(VI) stretching modes should allow a better view of the U═O bond during uranyl(VI) hydrolysis: weakness, symmetry changes, etc. For this purpose, we determine here new vibrational, IR and Raman data in D_2O and in basic H_2O solutions. As far as possible, both vibrational spectra were recorded in the same solution to allow a direct comparison. Structural data on uranyl(VI) complexes are completed by UV−visible electronic absorption spectroscopic measurements. The absorption intensity, band position, and band shift strongly depend on the chemical composition and the structure of the uranyl(VI) hydroxide species (mononuclear and polynuclear species).[26−29] In the present work, Raman, IR-ATR, and UV−visible electronic absorption spectra were therefore recorded to detect and characterize uranyl(VI)-hydrolyzed species over a wide $-\log mH(D)^+$ range using the organic noncomplexing base tetraethylammonium hydroxide, which does not interfere in the spectral region of the uranyl(VI) stretching bands. However, because the uranyl(VI) stretching bands strongly overlap, decomposition of a large set of spectra was difficult. To analyze our experimental data, a computational statistical method is therefore useful. Because some of the Raman spectra are noisy, the Bayesian Positive Source Separation (or BPSS) curve resolution method was chosen to analyze and to interpret our experimental data. This method was used to estimate the spectra of individual species from the whole vibrational spectra recorded in H_2O and D_2O basic media. The BPSS method[30−32] gives an estimation of the unknown component spectra and the concentrations of the underlying species. Where spectroscopic techniques fail to resolve unknown or unstable individual constituents contained in multicomponent mixtures, vibrational spectroscopies combined with BPSS treatment may offer a promising and efficient approach.[30−34]

EXPERIMENTAL SECTION

Materials. An acidic uranyl(VI) nitrate stock solution in H_2O was prepared from recrystallized schoepite, $[(UO_2)_8O_2(OH)_{12}](H_2O)_{12}$, by dissolution in a HNO_3 aqueous solution. The uranium concentration in this stock solution was determined using a gravimetric method: a weighed amount of the uranyl(VI) stock solution was first carefully evaporated to dryness and then transformed into U_3O_8 by heating to 800 °C for 48 h. The uranium concentration was determined from a weighed amount of U_3O_8 formed with an uncertainty of ±0.001 M. The concentration of the stock solution of uranyl(VI) was determined to be 0.506 M (U_{total}).

Tetramethylammonium hydroxide (TMAOH; 25 wt % in H_2O) and tetraethylammonium hydroxide (TEAOH; 20 wt % in H_2O) were purchased from Acros Organics and used as received.

TEAOD powder for basic solutions in D_2O was obtained as follows. The commercial TEAOH solution was heated at 100 °C for 48 h. The powder obtained was diluted in D_2O (99.9% D, Euriso-Top), and the solution was then dehydrated under vacuum for 48 h. This operation was repeated twice. The obtained dry powder was >90% deuterated and stored under vacuum until use.

Aqueous Uranyl(VI) Solutions. All solutions were prepared and handled in a nitrogen (99%) atmosphere glovebox containing NaOH pellets to minimize sample pollution by carbon dioxide.

Uranyl(VI) samples in H_2O with TEA-NO_3 or TMA-NO_3 electrolyte were obtained by mixing uranyl(VI) nitrate and TEAOH or TMAOH stock solutions. In strongly basic solutions, some uranyl(VI) samples were prepared by dissolution in a known amount of βUO_3 in concentrated 1−3 M TEAOH or TMAOH solutions. βUO_3 was synthesized by heating $UO_2(NO_3)_2 \cdot 6H_2O$ (Normapure, from Prolabo) to 452 °C.[35]

Uranyl(VI) samples in acidic D_2O with TEA-NO_3 electrolyte were obtained by heating to 100 °C the stock solution of uranyl(VI) nitrate in H_2O until an anhydrous powder was obtained. The salt was then dissolved in solutions of TEAOD in D_2O of different concentrations to get solutions at different $-\log mD^+$. Uranyl(VI) samples in basic D_2O solutions were obtained by the addition of βUO_3 in solutions of TEAOD in D_2O (1−3 M). Total dissolution was performed by mechanical agitation of tightly closed flasks for 5−15 days.

To obtain uranyl(VI) solutions free of all uranium particles, solutions were centrifuged at 10^4 rpm for 1 h before the spectroscopic study. The uranium concentration was then determined by the induced coupled plasma atomic emission spectroscopy method with a Perkin-Elmer Emission 2000 spectrometer. At 385.958 nm, uranium can be accurately analyzed in the concentration range 10^{-4}−5×10^{-3} M, with a relative uncertainty of 5%.

In $-\log mH^+ \leq 13$, the pH was measured using a Ross combination glass/reference electrode standardized against IUPAC buffers at pH 4, 7, and 12.45. Values of $-\log mD^+$ reported in the text are those read with the above-cited Ross electrode plus 0.4 units.[36] In highly basic solutions (pH > 13), $-\log mH^+$ values were determined as the effective OH^- molarity obtained from titration with standard HCl after subtraction of an amount of the hydrolyzed uranyl(VI) species, which was assumed to be entirely $UO_2(OH)_4^{2-}$. Under these conditions, $-\log mH^+$ values were determined within ±0.05 log unit.

Raman Spectra. Raman spectra were collected in the range 400−2000 cm^{-1} with a Jobin-Yvon ISA T64000 spectrometer. The instrument was equipped with a Notch filter to eliminate Rayleigh scattering, two kinds of gratings with 600 or 1800 grooves/mm, and a charged-coupled device (CCD) working at low temperature (140 K) with a 1024 × 256 pixels array. Samples were introduced in 10 mm square quartz cells. The excitation source was a home-modified SDL 8530-laser diode system (784.65 nm). It avoided fluorescence observed with excitation sources at lower wavelengths. The total radiant power of the scattering Stokes Raman spectra was recorded at 90° of both directions of incidence and of the polarization vector of the exciting laser beam. Wavenumbers were calibrated with the symmetric breathing mode of CCl_4 at 459 cm^{-1} with a precision better than 1 cm^{-1}. To overcome some problems of weak overlap of the TEAOH C−C and O═U═O

stretching bands below 800 cm^{-1} (see the Supporting Information), subtraction of pure TEAOH solution spectra from those containing uranyl(VI) species was performed until the C−N stretching bands at 894 and 904 cm^{-1} were canceled.

Curve resolution of Raman profiles in the rough was achieved with Gaussians using a converging self-consistent process for spectra of basic solutions using the Microcal Origin Peak Fitting Module for Windows. Each given hydrolyzed uranyl(VI) species was characterized by a distinct band located at one determined wavenumber $[\sigma(\nu_1)]$ of the symmetric stretching mode and having one constant full width at half-height (fwhh) over the whole series of Raman spectra. The first decomposition started with a minimum set of bands. These data were used in the second decomposition. If the decomposition was not correct (e.g., the residual peak is higher than a fixed limit), the band positions in the second spectrum were slightly changed and the decomposition started again. If the decomposition was not correct with these changes, one band was added. The fwhh of the additional band must be close, within ±3 cm^{-1}, to that of previous components, and its $\sigma(\nu_1)$ value was chosen to minimize the residual peak. A new set of components was thus defined and used for decomposition of the whole series of spectra. Calculations were ended when the correct curve resolution was reached. This procedure may be discussed because broad, poorly resolved bands always can be decomposed into more bands than effectively present. However, this procedure allowed one to avoid any personal subjective estimation, and only four principal bands fitted all of the spectra well.

IR Spectra. ATR-FTIR spectra were recorded using a Fourier transform Bruker Vector 22 spectrometer. The interferometer was equipped with a KBr beam splitter and a deuterated triglycine sulfate thermal detector. A nine-reflection diamond ATR accessory (Durasampl*IR*, SensIR Technologies) with an incident IR beam at 45° was used for acquiring spectra of uranyl samples. The sampling frequency was 10 kHz. Spectral resolutions were 4 or 2 cm^{-1}. The best signal/noise ratio was obtained with 400 scans and a total accumulation time of about 8 min. The irradiance throughout the optical device in the absence of a sample was about 11% of the full signal (without the ATR device). Compartments containing the detector and the ATR accessory were purged by circulating dry, CO_2-free air from a Balston compressor. Measurement requires about 100 μL of the sample. IR spectra were obtained between 4000 and 700 cm^{-1} and were displayed in the absorbance scale corresponding to $\log(R_{reference}/R_{sample})$, where R is the internal attenuated reflectance collected at the output of the ATR device. No overlapping bands between uranyl(VI) stretching bands and TEAOH absorption bands occurred (see the Supporting Information). Curve fitting of the IR spectra of acidic solutions was performed in the Microcal Origin Peak Fitting Module. The Gaussian band shape was sufficient to resolve the spectra.

UV−Visible Electronic Absorption Spectra. UV−visible electronic absorption spectra were recorded with an UV−visible Cary 5 spectrophotometer. The instrument was equipped with a double-beam ratio recording, a double out-of-plane Littrow monochromator, a 2 × 400 mm focal length, a dual double-sided grating with 1200 grooves/mm, a high-speed nonmeasurement-phase-stepping wavelength drive, a tungsten halogen bulb as the visible light source and a deuterium arc as the UV source, a beam splitting system with a chopper (30 Hz), and a R928 photomultiplier tube detector. Uranyl(VI) samples with TMAOH-NO_3 electrolytes were contained in 10-mm-path-length polystyrene cells, which do not absorb between 300 and 800 nm. Spectra of solutions using TEAOH with equivalent added quantities of OH^- have similar features. Only spectra with TMAOH are presented here for a direct comparison with those of Clark et al.[5] Absorption spectra were recorded between 300 and 550 nm with an accuracy of ±0.1 nm. The spectral resolution was 1.5 nm.

MCR with BPSS. The vibrational spectra of uranyl solutions are considered to be a weighted sum of the individual spectra (or pure spectra) of each complex species (or component) in the mixture. This mixing model assumes that m measured data $\{D_{(i,k)}, k = 1, ..., n\}_{i=1}^{m}$ from an evolving system are linear combinations of p unknown pure-component spectra $\{S_{(i,k)}, k = 1, ..., n\}_{i=1}^{p}$. Mathematically, this model is expressed as $D_{(i,k)} = \sum_{j=1}^{p} C_{(i,j)} S_{(j,k)} + E_{(j,k)}$, where $i = 1, ..., m$ and $j = 1, ..., p$; i and j index the measured spectra and the unknown pure-component spectra, respectively, and index k corresponds to the spectral variable $\{\lambda_k, k = 1, ..., n\}$. Each mixing coefficient $C_{(i,j)}$ is proportional to the concentration of the jth pure component in the ith mixture. The additive noise terms $\{E_{(i,k)}, k = 1, ..., n\}_{i=1}^{m}$ represent measurement errors and model imperfections. Using matrix notation, this model is written as $\mathbf{D} = \mathbf{SC} + \mathbf{E}$, where row vectors of the $m \times n$ data matrix $\mathbf{D}$ contain the m measured spectra and $\mathbf{C}$ is the $m \times p$ mixing matrix, with its column vectors representing the concentration profiles of the pure components. $\mathbf{S}$ is the $p \times n$ matrix, with its row vectors containing the p pure-component spectra, and $\mathbf{E}$ is the $m \times n$ noise matrix. By assuming a known number of components, mixture analysis (also called multivariate curve resolution or MCR) can estimate the pure-component spectra $\mathbf{S}$ and the mixing coefficient profiles $\mathbf{C}$ from the mixture spectra $\mathbf{D}$ without any a priori information. The BPSS method developed recently in our group addresses the mixture spectra decomposition using Bayesian estimation theory and Markov chain Monte Carlo (MCMC) under nonnegativity constraints on both the concentration and spectra.[30−33] The main idea is to first construct the posterior probability distribution function (pdf) of the pure-component spectra and their concentrations. According to Bayes' theorem, computation of this pdf needs to specify a statistical model for the mixing model (linear mixing with Gaussian measurement errors) and for the pure spectra and concentration profiles (an appropriate pdf that encodes nonnegativity and sparseness). A second step is to jointly estimate the pure spectra and the concentration profiles from this posterior law (pdf) using MCMC methods. The MCMC methods generate possible solutions for a target pdf, which is the posterior law in our case. The use of this stochastic estimation technique precludes convergence to local minima and yields a method that works in an unsupervised framework with effective results even for high noise levels in a reasonable time. The only necessary parameters to tune are the number of components and the number of MCMC algorithm iterations. For more details on this approach, the reader is referred to refs 30−33.

Singular value decomposition (SVD) was used to estimate the rank of the data sets. The usual approximation is that the number of large singular values, significantly different in magnitude from the noise-related singular values, indicates the rank of the analyzed matrix. In principle, a successful separation can be achieved by using the appropriate number of components. An advantage of BPSS is that the number of components can be introduced into the algorithm and several trials can be conducted within minutes until the error matrix does not carry recognizable spectral features. Thus, the number of components may be chosen from SVD, but it is ultimately the algorithm that shows whether the number of requested components is correct.

The closure constraint can be applied to closed systems of the reaction, where the principle of mass balance is fulfilled. With this constraint, the sum of the concentrations or fractions of all of the species involved in the reaction or mixture (the suitable elements in each row of the $\mathbf{C}$ matrix) is forced to be equal to a constant value (the total concentration or fractions) at each stage in the reaction or in the mixture.[31,33,34] In the studied systems, the fraction of each uranyl structure was sought. Therefore, for each uranyl system, the sum of the fractions of the uranyl complexes is equal to 1. Baselines for all spectra presented in this work were adjusted to zero using linear functions. Because the BPSS algorithm is well suited to work with noisy signals, we preferred not to alter our raw spectra by a smoothing or denoising procedure even when spectral series were very noisy. The reconstruction quality of each pure spectrum or concentration profile is assessed using a measure of dissimilarity between their recovered and reference values. Note that use of the dissimilarity measure is possible only when the reference spectra are available in an evaluation framework

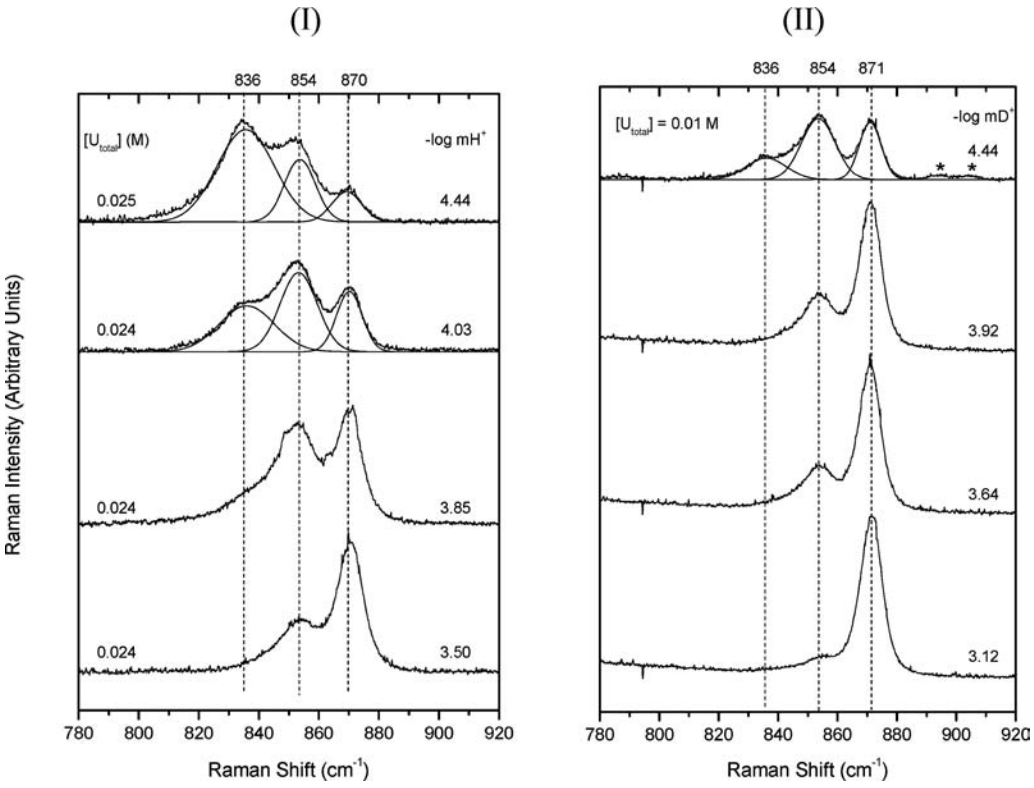

Figure 1. Raman spectra (I) in H_2O and (II) in D_2O of $(C_2H_5)_4NNO_3$/uranyl(VI) aqueous solutions. U_{total} (M), $-\log mH^+$, and $-\log mD^+$ values are indicated on the figures. Offsets of the spectra are used for clarity. Decomposed bands are also plotted for three representative compound spectra. Asterisks indicate scattering bands from the tetraethylammonium cation.

of the methods. Otherwise, a criterion such as the lack of fit (LOF) can be used to assess how the estimated pure spectra and mixing coefficients can reproduce the observed data. However, it does not measure how well the spectra and concentration profiles are estimated. The percentage LOF and explained variance (R^2) values are calculated by using of the following equations:

$$\mathrm{LOF} = \sqrt{\frac{\sum_i \sum_k (d_{i,k} - \hat{d}_{i,k})^2}{\sum_i \sum_k d_{i,k}^2}}$$

$$R^2 = \frac{\sum_i \sum_k \hat{d}_{i,k}^2}{\sum_i \sum_k d_{i,k}^2}$$

$d_{i,k}$ and $\hat{d}_{i,k}$ are the elements of **D** and the elements of the reconstructed matrix by the BPSS model, respectively. It is important to bear in mind that R^2 is highly dependent on the noise level of the data. Because some of our data are very noisy, the explained variance resulting from resolution of these data is often lower than 95%. In this paper, the BPSS results are presented in two forms: (1) the normalized estimated pure spectra of individual species and (2) the estimated relative concentration of each individual species against $-\log mH(D)^+$.

MATLAB 7.1 (The Mathworks, Natick, MA) and the BPSS code were used for all calculations. The BPSS code is available upon request.

RESULTS

1. Raman spectra. Figures 1 and 2 show the decrease of the symmetric stretching mode wavenumber of hydrolyzed uranyl(VI) species as $-\log mH^+$ and $-\log mD^+$ increase from 3.50 to 14.38 and from 3.12 to 13.34, respectively. In acidic solutions, Raman spectra clearly show three scattering bands at the same wavenumbers whatever solvent was used, H_2O or D_2O (Figure 1). The results in H_2O are in agreement with those reported in previous studies.[2,9,10] The reported wavenumbers and fwhh's are gathered in Table 1. In basic solutions, Raman spectra display poorly resolved bands (Figure 2), with a maximum that shifted from about 815 cm^{-1} to about 780 cm^{-1} as $-\log mH^+$ and $-\log mD^+$ increased. The results in H_2O were in accordance with the Raman general spectral features obtained in uranyl(VI) tetramethylammonium solutions in H_2O, except for the strong overlapping bands in the 740−800 cm^{-1} region.[9] The high shift (>30 cm^{-1}) of the broad bands was indicative of the presence of more than one single band, and therefore of the occurrence of several uranyl(VI) species.

2. ATR-FTIR Spectra. Because of the strong absorption of liquid water below 900 cm^{-1}, spectra in H_2O were quite "noisy". On the contrary, spectra in D_2O had good signal-to-noise ratios. Figures 3 and 4 show the shifting of the antisymmetric stretching mode of hydrolyzed uranyl(VI) species from about 960 to about 830 cm^{-1} as $-\log mH^+$ and $-\log mD^+$ increase from 2.52 to 14.43 and from 3.12 to 13.34, respectively. In H_2O acidic solutions, spectra of uranyl(VI) show up to three bands (Figure 3(I)). Wavenumbers and fwhh's are gathered in Table 1. These results are in accordance with the previously published results.[10] In D_2O, spectra also show up to three bands that are better resolved. They were shifted to lower wavenumber with respect to the bands observed in spectra for similar samples in H_2O. Indeed, the uranyl(VI) bands in D_2O samples absorbed at

dx.doi.org/10.1021/ic101953q |*Inorg. Chem.* 2011, 50, 2811–2823

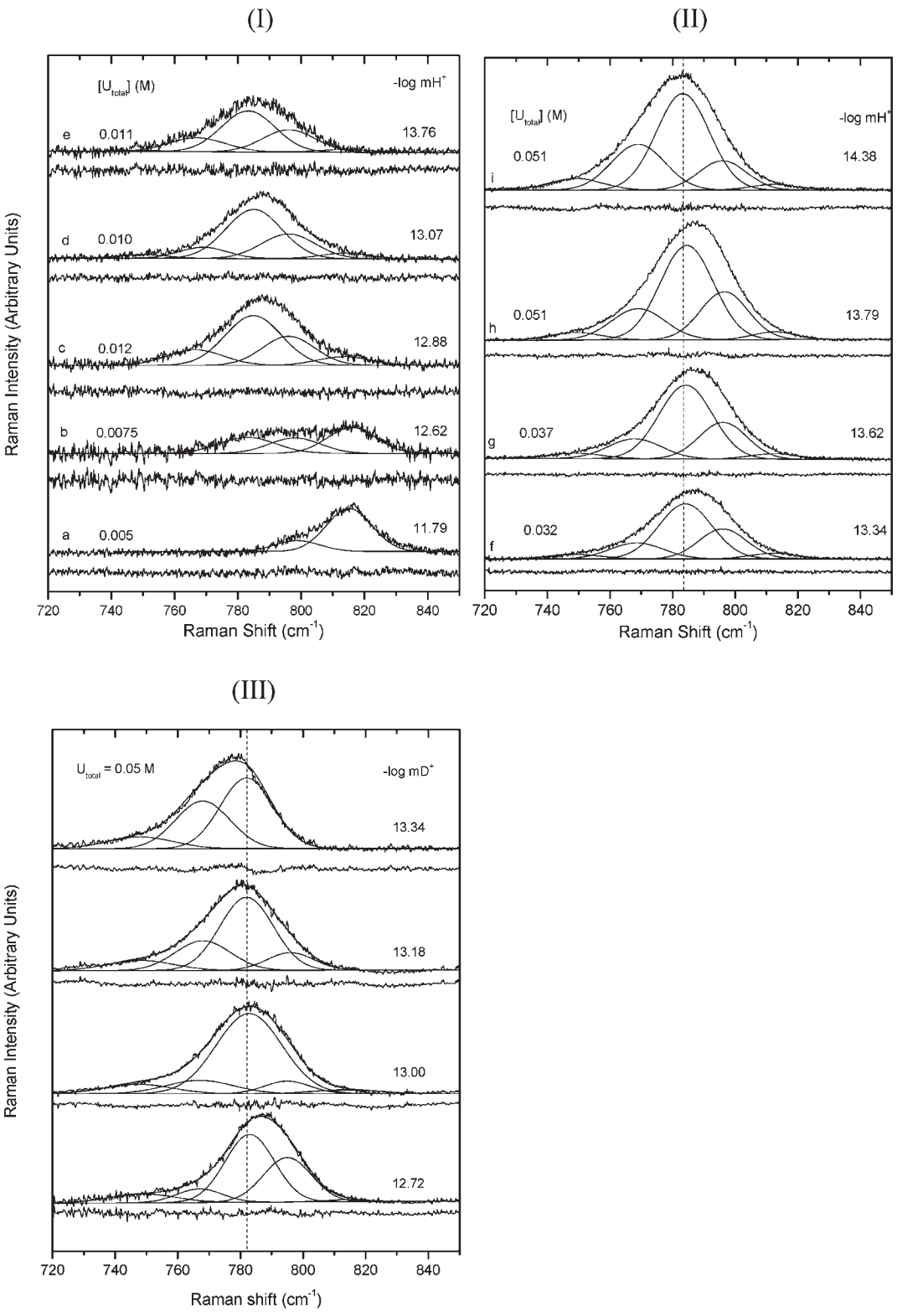

Figure 2. Raman spectra with decomposed bands and residual peaks of aqueous solutions of $(C_2H_5)_4NNO_3$: (I and II) in H_2O; (III) in D_2O. U_{total} (M), $-\log mH^+$, and $-\log mD^+$ values are indicated on the figures. Offsets of the spectra are used for clarity.

6−10 cm^{-1} lower values, and the mean fwhh value was half compared to the one observed in H_2O (Table 1). In basic solutions, except for a better signal-to-noise ratio in D_2O, roughly similar spectral features were observed (Figure 4). Broad, poorly resolved bands that shifted from 915 cm^{-1} to about 835 cm^{-1} were observed as $-\log mH^+$ and $-\log mD^+$ increased. The high band shift (≈80 cm^{-1}) shows again that several bands, i.e., several uranyl(VI) species, coexist. This result was consistent with the Raman spectra of the uranyl(VI) species in basic solutions presented above. Absorption bands were determined

dx.doi.org/10.1021/ic101953q |*Inorg. Chem.* 2011, 50, 2811–2823

Table 1. Wavenumber Values (cm^{-1}), fwhh's (cm^{-1}), and Tentative Assignments of the Vibrational UO_2 Symmetric (ν_s) and Antisymmetric (ν_a) Stretching Bands[a]

	Raman								IR							
	H_2O				D_2O				H_2O				D_2O			
	Dcp				Dcp				Dcp				Dcp			
uranyl(VI) species	ν_s	fwhh	ν_s	fwhh	ν_s	fwhh	ν_s	fwhh	ν_a	fwhh	ν_a	fwhh	ν_a	fwhh	ν_a	fwhh
								Acidic Medium								
(1,0)	870	11			871	10			962	23			953	9		
(2,2)	854	13			854	13			943	25			936	14		
(3,5)	836	23			836	16			923	30			916	16		
	Raman								IR							
	H_2O				D_2O				H_2O				D_2O			
	Dcp		BPSS		Dcp		BPSS		Dif		BPSS		Dif		BPSS	
uranyl(VI) species	ν_s	fwhh	ν_s	fwhh	ν_s	fwhh	ν_s	fwhh	ν_a	fwhh	ν_a	fwhh	ν_a	fwhh	ν_a	fwhh
								Basic Medium								
(3,8)	815	17	815	20	815				915		916	22				
(3,11)	797	17	793	22	796		790	22	873		868	32	868		854	30
(1,4)	784	20	782	23	782				857				854			
							777	25			845	42			843	39
(1,5)	767	20	765	30	768				835				834			
(1,6)	748	20														

[a] Dcp: results from decomposition of the spectra. BPSS: results from BPSS calculations. Dif: results from the difference spectra.

by using difference spectra between successive IR-ATR spectra (Figure 4). Bands at 873, 857, and 835 cm^{-1} and at 868, 854, and 834 cm^{-1} were determined from spectra of samples in H_2O and D_2O, respectively.

3. BPSS Analysis of Vibrational Spectra. This procedure of curve resolution, which allowed avoidance of any personal subjective estimation, was used to help interpretation of the spectra in basic media where stretching bands of uranyl(VI) species strongly overlap. The data processing was applied to 26 Raman spectra in H_2O, 7 Raman spectra in D_2O, 17 IR-ATR spectra in H_2O, and 11 IR-ATR spectra in D_2O (see the Supporting Information to have a whole view of the spectra). The BPSS analysis shown in Figure 5(I)A identified four compounds from the Raman spectra of the samples in H_2O and $-\log mH^+$ ranging from 12.18 to 14.38, and it includes 87% of the variance. Two pure spectra, which account for 96% of the spectral variance of the spectra set, were found with a shorter explored $-\log mD^+$ range from 12.72 to 13.84 [Figure 5(II)A]. In the $-\log mH^+$ range 12.62−14.38, three pure spectra were estimated from the IR-ATR spectra, and they account for 88% of the spectral variance [Figure 5(I)B]. Two pure spectra, which account for 94% of the spectral variance of the IR-ATR spectra set, were found within the explored $-\log mD^+$ range 12.72−13.84 [Figure 5(II)B]. Because of some asymmetry of the band at low wavenumber [Figure 5(II)A,B], a third pure spectrum could be expected; however, the program did not converge if three principal components were imposed. For all of the spectra examined, the percentage of nonreconstructed data was mainly noise, indeed, some spectra with low uranyl(VI) concentrations were quite noisy (see the Supporting Information). The results including wavenumbers and fwhh's for pure estimated spectra are summarized in Table 1.

Figures 6 and 7 show the concentration profiles against the $-\log mH(D)^+$ values of the samples analyzed calculated by BPSS. In H_2O, where four species were found in the Raman spectra, species scattering at 815 cm^{-1} rapidly decreases with an increase of $-\log mH^+$ (Figure 6A). The same feature was observed for the species absorbing at 916 cm^{-1} in the IR-ATR spectra (Figure 6B). The concentration of the species characterized by a scattering band at 793 cm^{-1} and an absorbing band at 868 cm^{-1} drastically increases above $-\log mH^+ = 12.5$, stayed almost constant until $-\log mH^+ = 13.7$, and tended to decrease above $-\log mH^+ = 14$. Finally, the concentration of the species absorbing at 845 cm^{-1} smoothly increases between $-\log mH^+$ values 12.6 and 14.4 (Figure 6B). The concentration of the species scattering at 782 and 765 cm^{-1} had the same evolution as the latter IR band. Moreover, if one plots the sum of both concentrations estimated from the Raman spectra at 782 and 765 cm^{-1} as a function of $-\log mH^+$, evolution was very similar to that for the species absorbing at 845 cm^{-1} (data not shown). In D_2O, evolution of the estimated concentrations of both species is simple: the concentration of the species with the band at the higher wavenumber decreased with an increase of $-\log mD^+$, whereas that at the lower wavenumber increased for both types of vibrational spectra (Figure 7). However, some differences in the evolution of the concentrations can be noticed. Indeed, whereas the concentrations of both species are equal from the IR spectra at $-\log mD^+ < 13$, they are not from the

dx.doi.org/10.1021/ic101953q |Inorg. Chem. 2011, 50, 2811–2823

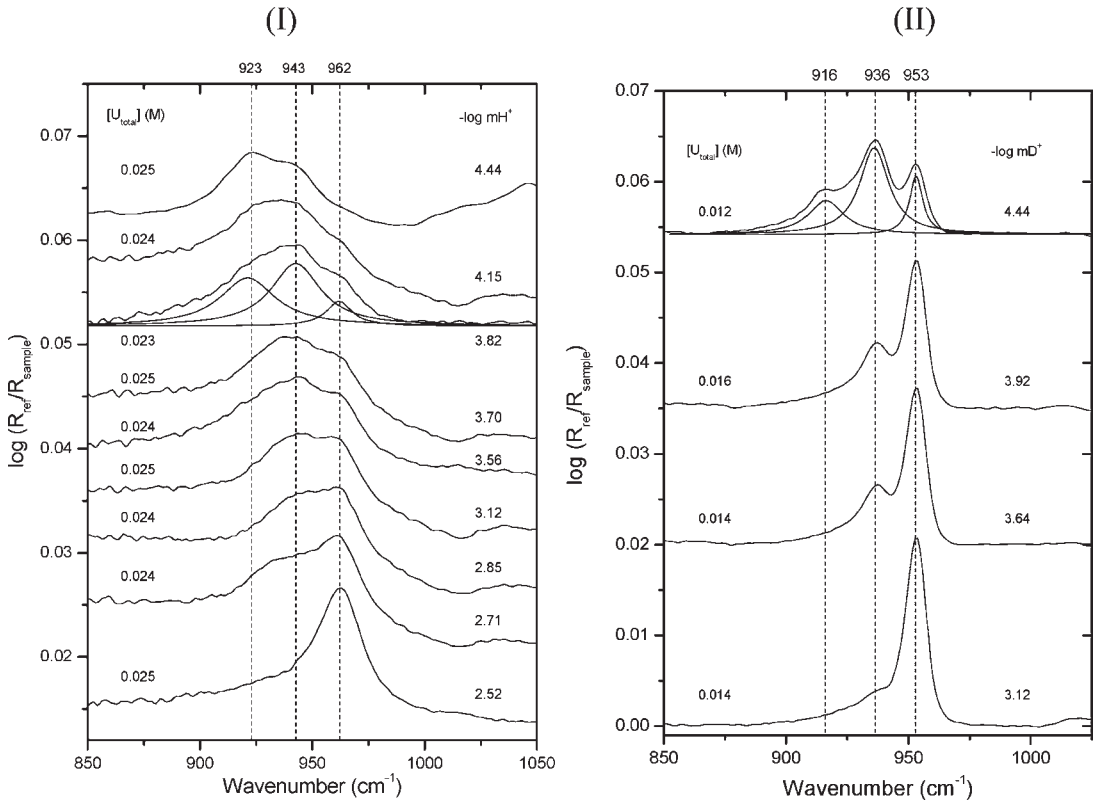

Figure 3. ATR-FTIR spectra of $(C_2H_5)_4NNO_3$/uranyl(VI) aqueous solutions (I) in H_2O and (II) in D_2O. U_{total} (M), $-\log mH^+$, and $-\log mD^+$ values are indicated on the figures. Offsets of the spectra are used for clarity. Decomposed bands are also plotted for three representative compound spectra.

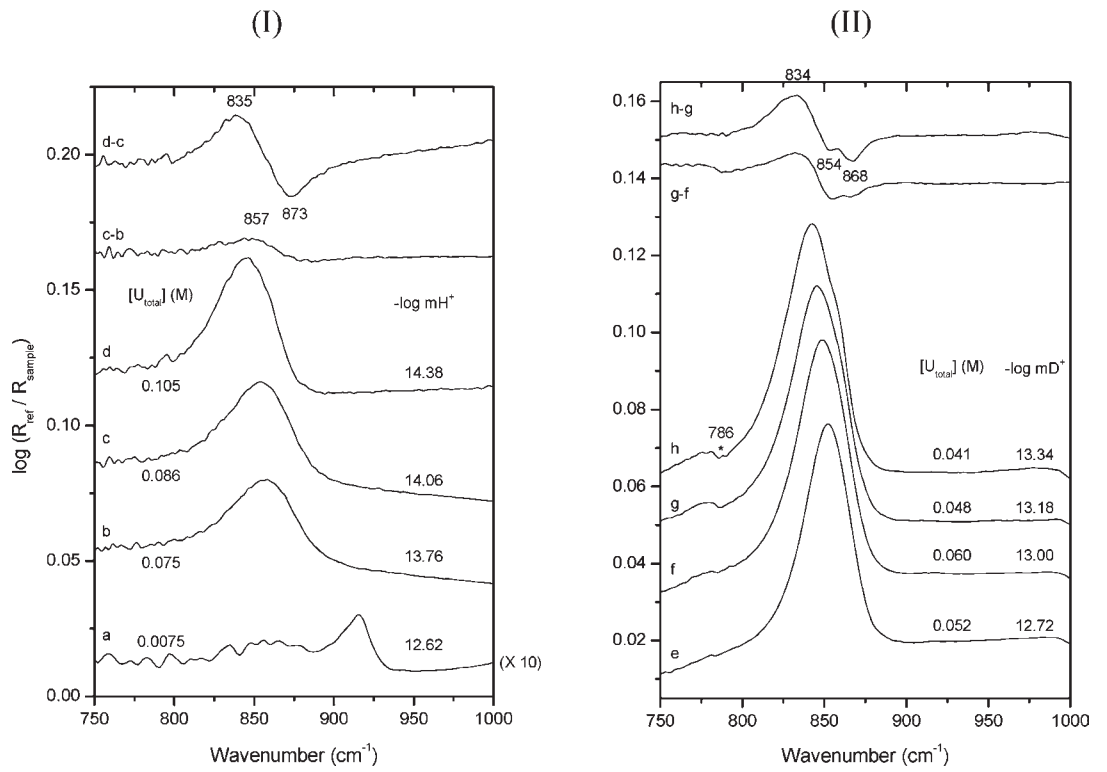

Figure 4. ATR-FTIR spectra and difference plots of IR spectra of $(C_2H_5)_4NNO_3$/uranyl(VI) aqueous solutions (I) in H_2O and (II) in D_2O. U_{total} (M) and $-\log mH(D)^+$ values are indicated on the figures. c-b is the difference between spectra c and b, and d-c is the difference between spectra c and b. Offsets of the spectra are used for clarity. (*) This spectral feature is due to a lack of TEAOD subtraction.

dx.doi.org/10.1021/ic101953q |*Inorg. Chem.* 2011, 50, 2811–2823

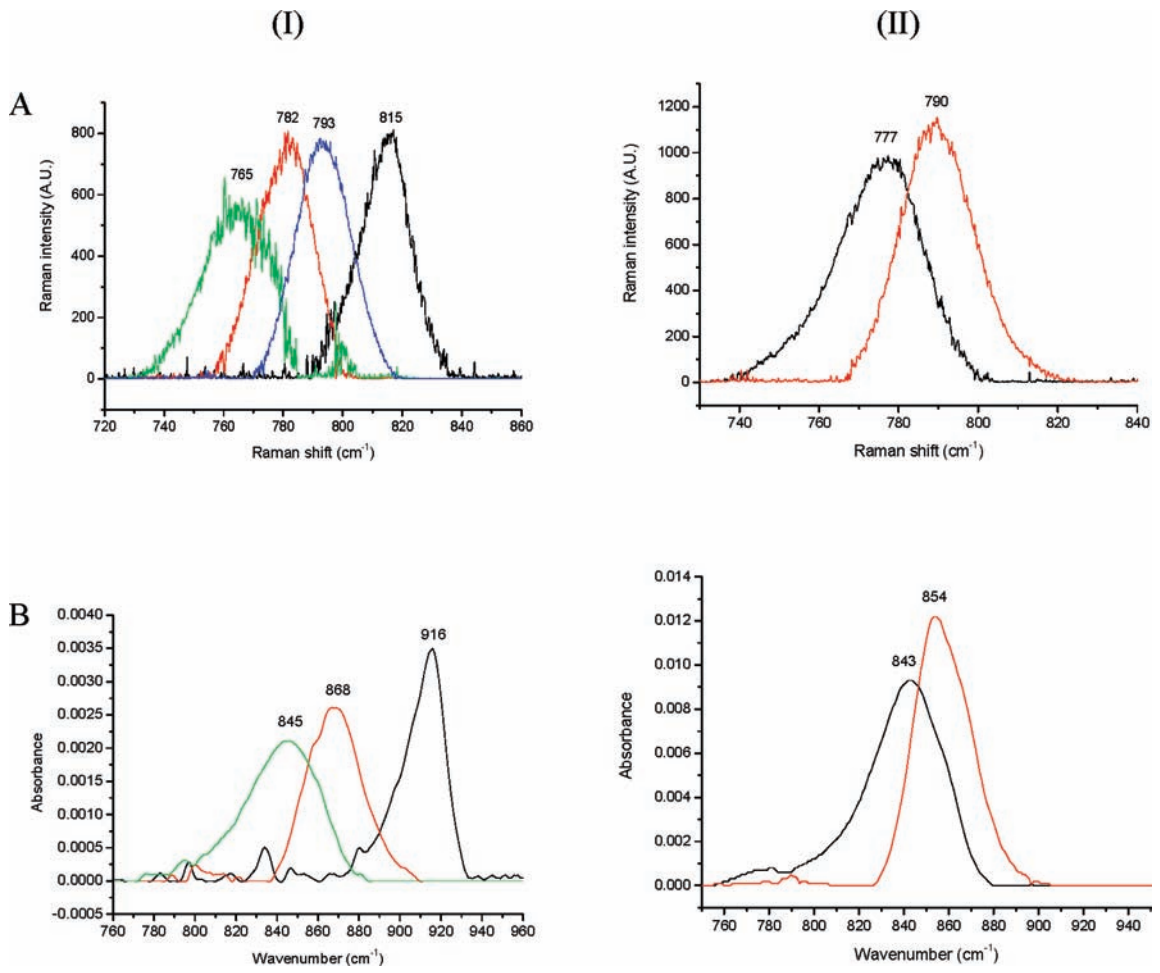

Figure 5. Estimated BPSS (A) Raman and (B) IR-ATR pure spectra for species in basic solutions (I) in H_2O and (II) in D_2O.

Raman data. These differences are probably a consequence of the nonidentical modification of stretching vibrations by complexation in D_2O, which make a direct comparison of the IR and Raman signals difficult.

4. UV−Visible Electronic Absorption Spectra. Figure 8 shows UV−visible absorption spectra from the whole $-\log mH^+$ range investigated in the present study. A spectrum with the lowest absorption, a good band definition, and the main absorption band, $\lambda_{max} \approx 414$ nm, was recorded for UO_2^{2+} in an acidic solution (Figure 8a). An increase of $-\log mH^+$ from 2.92 to 4.11 leads to a significant increase of the absorption intensity, a change in the band shape with a poor band definition, and a red shift of the main absorption band, $\lambda_{max} \approx 420$ nm (Figure 8b,c). These features were in accordance with other published spectra.[28] The spectrum recorded at $-\log mH^+ = 11.36$ displays a poor band definition and a maximum red shift with a main absorption band at 430 nm (Figure 8d). A decrease in the absorption was observed as $-\log mH^+$ increased from 11.36 to 12.14 (Figure 8d,e). A high absorption decrease with a slight blue shift occurred as $-\log mH^+$ increased from 12.14 to 12.79 (Figure 8e,f). At $-\log mH^+ = 13.68$, the absorption bands were blue-shifted to $\lambda_{max} \approx 400$ nm. The maximum intensity was lower, and the band definition was higher (Figure 8g). In highly basic solutions, the absorption feature exhibited small, monotonic shifts to longer wavelengths and higher intensity with increasing $-\log mH^+$ from 13.68 to 14.50 (Figure 8g,h). It was indicative of the formation of new species. The spectral features at $-\log mH^+ > 13$ were in accordance with published spectra of similar uranyl(VI) solutions.[5]

DISCUSSION

1. Species in Acidic Solutions. Uranyl(VI) species in acidic solutions are well-known. The three {Raman; IR-ATR} band couples with decreasing wavenumbers at {870; 962}, {854; 943}, and {836; 923} cm^{-1} were assigned in accordance with our previous work[10] to species UO_2^{2+} [hereafter called (1,0)], $(UO_2)_2(OH)_2^{2+}$ [hereafter called (2,2)], and $(UO_2)_3(OH)_5^{+}$ [hereafter called (3,5)], respectively (Table 1). The TEAOH base was then confirmed to be noncomplexing because wavenumbers were equal to those recorded in other media. The dimer and trimer should have structures similar to those determined by X-ray in concentrated solutions.[37,38] The U−U interactions were shown by EXAFS measurements.[7] The occurrence of polynuclear species was also confirmed by the UV−visible spectra principally with an increase of the molecular absorption coefficient with respect to that of the monomeric hydrated species.[26,28] By comparison with the results obtained in H_2O, the three {Raman; IR-ATR} band couples with decreasing wavenumbers at {871; 953}, {854; 936}, and {836; 916} cm^{-1} reported for samples in D_2O were easily assigned to species UO_2^{2+}, $(UO_2)_2(OD)_2^{2+}$, and $(UO_2)_3(OD)_5^{+}$, respectively (Table 1).

dx.doi.org/10.1021/ic101953q |*Inorg. Chem.* 2011, 50, 2811–2823

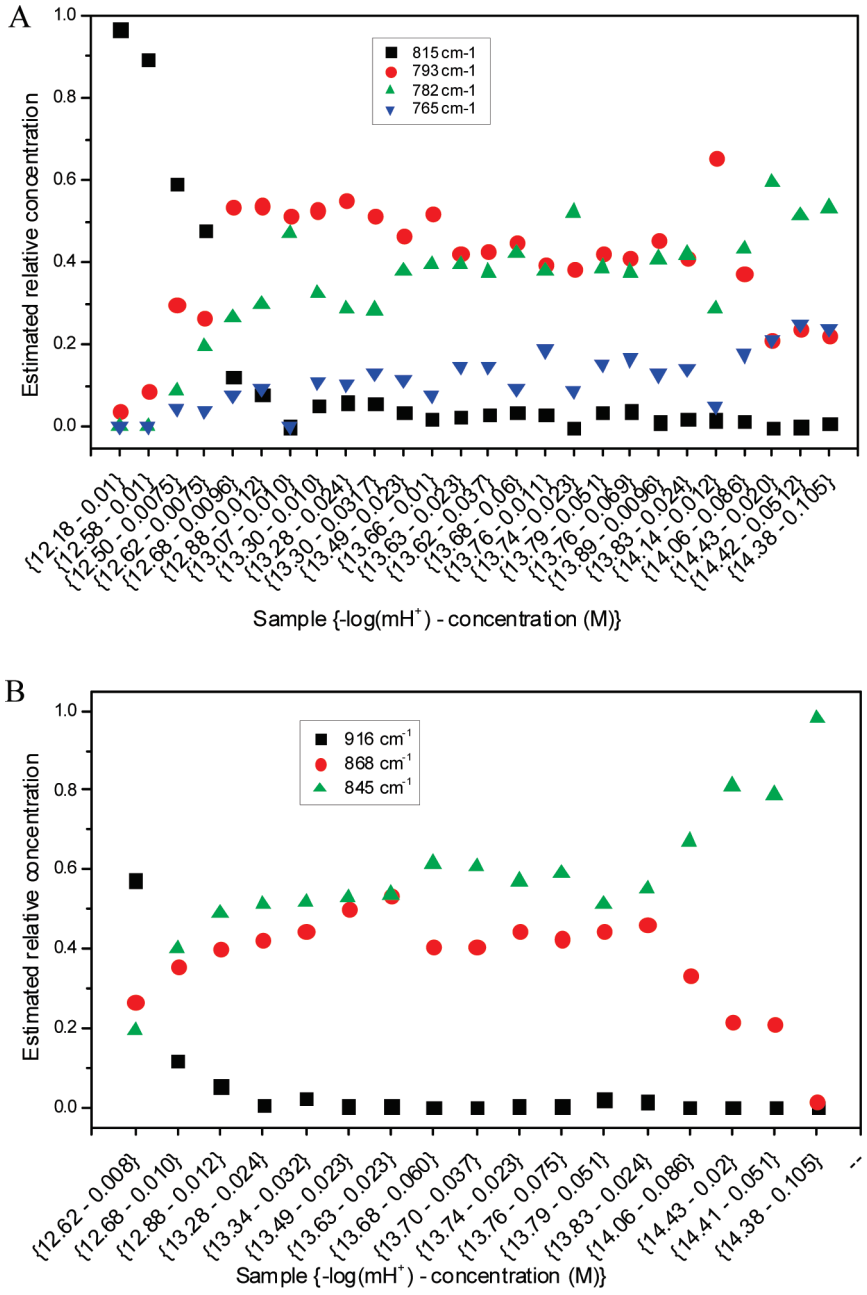

Figure 6. Estimated concentration profiles of uranyl(VI) species in basic solutions in H_2O by BPSS: (A) from the Raman spectra; (B) from the IR-ATR spectra. Key for the abscissa axes: Samples are presented with increasing {−log mH^+ − uranyl total concentration (M)} values.

The presence of three species showed that the nature of the complexes was not affected by the replacement of H_2O with D_2O. All species were also characterized by only one active Raman band and only one active IR band. However, whereas the Raman symmetric stretching bands were unchanged, IR antisymmetric stretching bands absorbed at lower wavenumbers and were narrower. The shift was the highest for species (1,0), and it was lower for species (2,2) and (3,5) (Table 1). It can then be linked to the number of water molecules in the different complexes, that is, five, three, and two for complexes (1,0), (2,2), and (3,5), respectively. However, a simple mass effect was not enough to explain this result because Raman scattering bands remained unchanged. The uranium atom and water molecules do not move in the symmetrical stretching mode, whereas they do move in the antisymmetric stretching mode. The observed wavenumbers could be explained by a mechanical coupling with water molecules due to intermolecular interactions that are negligible for the symmetric stretching mode and high for the antisymmetric stretching mode. Evidence of this would only be given by a complete normal-coordinate analysis for all of the suggested species. In addition, the lower fwhh values for individual bands in spectra recorded in D_2O were probably either also due to the above-cited mechanical coupling with water molecules and/or due to a lower number of water molecule exchanges that might be slower in D_2O.

2. Highly Basic Solutions (−log $mH^+ \geq 13.70$). Only spectra in H_2O were obtained. Spectra were assigned by comparison to published data provided by EXAFS and ^{17}O NMR in comparable

dx.doi.org/10.1021/ic101953q |*Inorg. Chem.* 2011, 50, 2811–2823

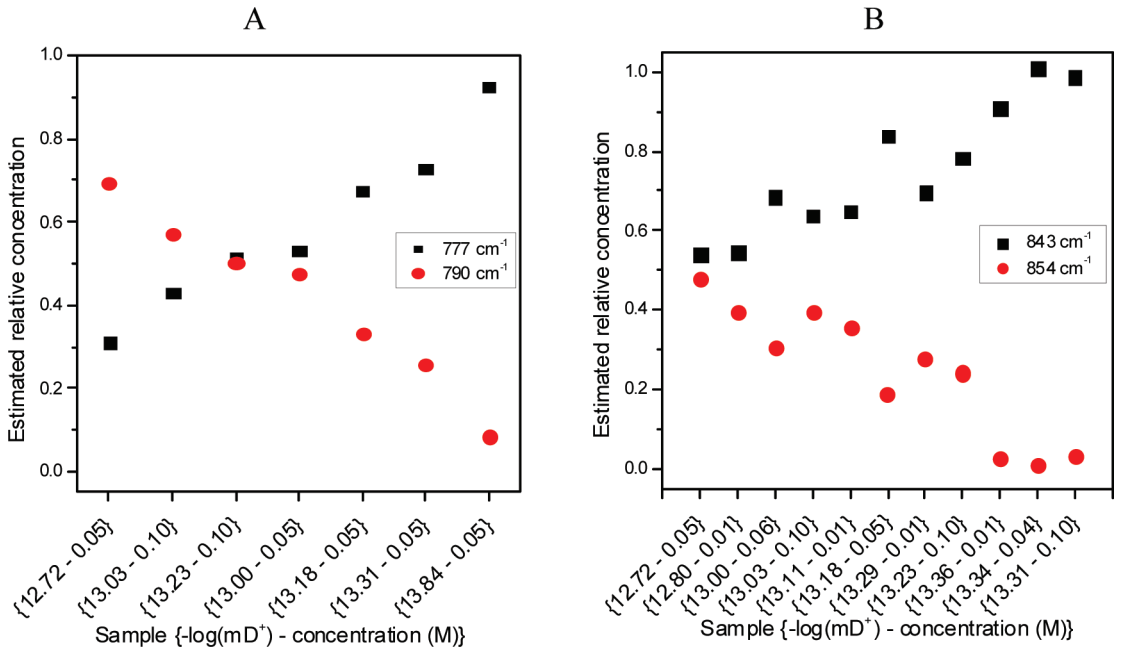

Figure 7. Estimated concentration profiles of uranyl(VI) species in basic solutions in D_2O by BPSS: (A) from the Raman spectra; (B) from the IR-ATR spectra. Key for the abscissa axes: Samples are presented with increasing {−log mH^+ − uranyl total concentration (M)} values.

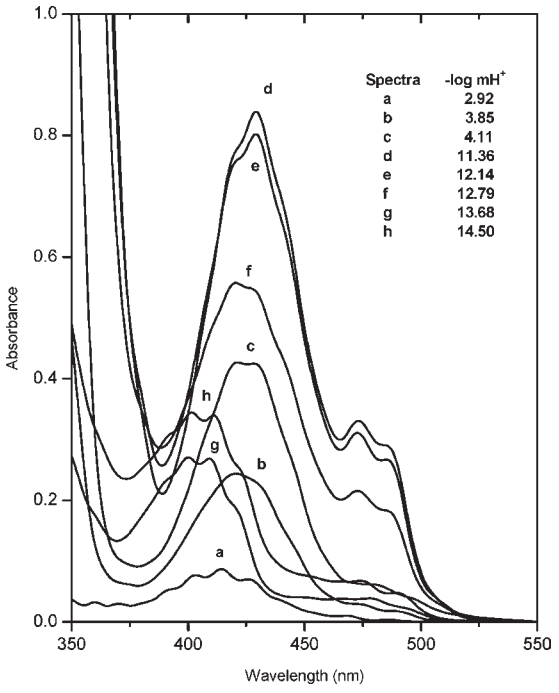

Figure 8. UV−visible electronic absorption spectra of $(CH_3)_4NNO_3$/uranyl(VI) aqueous solutions in H_2O. The U_{total} value is 0.01 M, and −log mH^+ values are indicated on the figure.

solutions.[5−7] Three major bands occurred in the Raman spectra. The concentration of the species scattering at 782 cm^{-1} was the highest at −log $mH^+ \geq 14$. The integrated intensity of the band at 793 cm^{-1} tended to decrease at −log $mH^+ > 14$, whereas that of the band at 765 cm^{-1} increased (Figure 6A). At similar −log mH^+ values, EXAFS measurements indicated that the number n of OH^- ligands coordinated to the uranium atom of the uranyl(VI) group of hydrolyzed species increased from 4.2 to 5.3 as −log mH^+ increased from 13.40 to 14.50.[5−7] In a 0.5 M TMAOH solution (−log mH^+ = 13.40), the value n = 4.2 clearly indicates that the major species should be monomer $UO_2(OH)_4^{2-}$ [hereafter called (1,4)].[7] The band at 782 cm^{-1} was therefore assigned to species (1,4). Previous works[1,5] already showed a broad band at 786 cm^{-1} in 3.5 M TMAOH solutions of uranyl(VI) that was assigned to (1,4). In 1.0−3.5 M TMAOH solutions (−log mH^+ = 13.7−14.5), n was in the range 4.6−5.3.[5−7] These values were interpreted as a result of an exchange reaction between monomers $UO_2(OH)_4^{2-}$ and $UO_2(OH)_5^{3-}$ [hereafter called (1,5)].[5,7] Because the area of the band at 765 cm^{-1} was the lone one to significantly increase in the same −log mH^+ range (Figure 6A), it was assigned to species (1,5). The UV−visible spectra obtained at −log mH^+ = 14.50 were characterized by significantly less intense bands compared to those of hydrolyzed triuranyl(VI) species, a good band definition, and a blue-shifted band with respect to the spectrum of the nonhydrolyzed monomer (Figure 8). These features indicated a higher symmetry of the uranyl environment, which implies a weaker transition. This suggests the occurrence of monomers, which are more symmetric than oligomers. Similar observations were already made in highly acidic solutions.[28] Our spectra are in accordance with spectra already published for highly basic uranyl solutions, where the occurrence of monomers was claimed.[5] One additional argument in favor of this assignment is the good agreement of the mole ratio, [(1,5)]/[(1,4)], reported by Moll et al.[7] of ca. 0.3 using ^{17}O NMR measurements and 0.3−0.4 determined from Raman spectral data in the present study. In the IR spectra, only three bands were estimated by BPSS analysis, the algorithm did not converge when one additional component was imposed. However, the concentration profile of the resolved band at 845 cm^{-1} was very close to the profile of the sum of species concentrations of estimated bands at 782 and 765 cm^{-1} in the Raman spectra. The wavenumber of this BPSS estimated band was at the middle of the two bands at 857 and 835 cm^{-1} obtained in the difference spectra [Figure 4(I)]. The BPSS estimated band

dx.doi.org/10.1021/ic101953q |*Inorg. Chem.* 2011, 50, 2811–2823

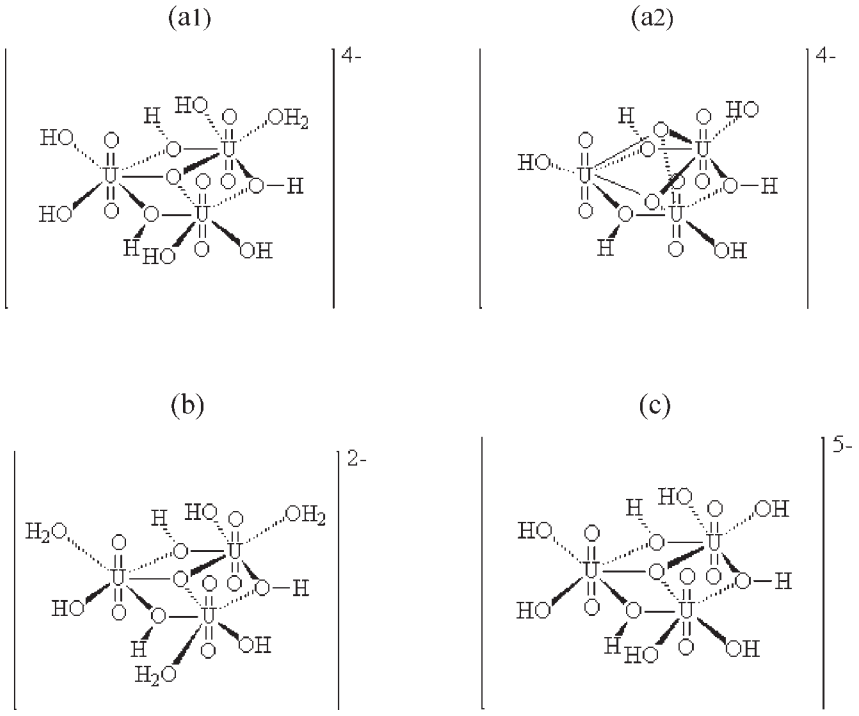

Figure 9. Possible structures of the three trimers: (a1 and a2) $(UO_2)_3(OH)_{10}^{4-}$, (b) $(UO_2)_3(OH)_8^{2-}$, and (c) $(UO_2)_3(OH)_{11}^{5-}$.

at 845 cm^{-1} should thus be composed of two bands centered at 857 and 835 cm^{-1} [Figure 4(I)], and they were assigned to species (1,4) and (1,5), respectively. Müller et al.[18] also observed IR broad, poorly resolved bands centered at 870 cm^{-1} in a TMAOH basic medium. Although assigned to a lone species (1,4), several bands probably occurred in these broad, poorly resolved bands. The decomposition of Raman spectra of highly basic solutions ($-\log mH^+ \geq 13.7$) indicated the presence of a minor species with a band at 748 cm^{-1} (Figure 2). The BPSS method did not resolve this band. However, the BPSS resolved band at 765 cm^{-1} has a higher fwhh than the others (Table1) and was not symmetrical [Figure 5(I)A]. The value $n = 5.3$ determined in a 3.5 M TMAOH solution by Clark et al.[5] could correspond to the presence of the above two monomers and another species that is more hydrolyzed. The low absorption intensity in the corresponding UV−visible spectra (Figure 8h) is in favor of the occurrence of a monomer. All of these facts allowed us to suggest a species of formula $UO_2(OH)_6^{4-}$, where the uranyl(VI) group is equatorially surrounded by a hexagon of six OH^- ligands and would have D_{6h} symmetry. This assumption is based on the bidentate structure of solid and aqueous complex $UO_2(CO_3)_3^{4-}$ determined by X-ray diffractometric and optical (luminescence, IR absorption, and Raman scattering) spectroscopic studies.[39,40]

3. Moderate Basic Solutions ($12 < -\log mH^+ < 13$). As stated in the reference book by Guillaumont et al.,[15] identification of trimeric species in basic solutions with pH values below 13 and uranium concentrations above 10^{-4} M remains an unsolved problem. Since the publication of this book, we have not found any works dealing with the study of such basic solutions. Before discussing species in these solutions, one should note that the concentration values needed for vibrational spectroscopies are too high to obtain long-time stable solutions of uranyl at $-\log mH^+ \ll 12$. Therefore, the well established $(UO_2)_3(OH)_7^-$ complex[15] did not occur in the studied solutions, and it was not taken into account in the interpretation of the spectra.

Up to three bands occurred in the small range of 11.79−12.62 of $-\log mH^+$ [$0.005 \text{ M} \leq U_{total} \leq 0.0075$ M; Figure 2(I)]. The area of the band at 815 cm^{-1} decreased drastically, whereas that of the band at 793 cm^{-1} strongly increased with an increase of $-\log mH^+$. The integrated intensity of the band at 782 cm^{-1} tended to smoothly increase below $-\log mH^+ = 13$ (Figure 6A). The latter band was already assigned to species (1,4), and the evolution of the corresponding concentration is in agreement with the fact that this species is preponderant at the highest $-\log mH^+$ values. The band at 815 cm^{-1} was the most intense at the lowest $-\log mH^+$ value (Figure 6A). Besides, the IR spectrum recorded at $-\log mH^+ = 12.62$ ($U_{total} = 0.0075$ M) showed one major band at 916 cm^{-1} (Figure 6B). Both band intensities drastically decreased as the solution was enriched with OH^- ligands (Figure 6A,B) and were assigned to the same uranyl species. The intensity of the IR band at 868 cm^{-1} tended to decrease as $-\log mH^+$ increased (Figure 6B), as did the scattering band at 793 cm^{-1} (Figure 6A). Both vibrational bands were associated with the same species. Absorption UV−visible spectra recorded in similar experimental conditions ($11.36 \leq -\log mH^+ \leq 12.14$; $U_{total} = 0.01$ M; Figure 8d,e) showed the most intense absorption bands characterizing polyuranyl(VI) species. Consequently, the two {Raman; IR-ATR} band couples at {815; 916} and {793; 868} cm^{-1} were assigned to two oligomer species of uranyl(VI). From earlier works on the hydrolysis of uranyl(VI),[4,9] species $(UO_2)_3(OH)_8^{2-}$ [hereafter called (3,8)], $(UO_2)_3(OH)_{10}^{4-}$ [hereafter called (3,10)], and $(UO_2)_3(OH)_{11}^{5-}$ [hereafter called (3,11)] can be suggested in the present uranyl(VI) concentration range. However, there are only two vibrational bands. Structural considerations will solve this problem. Triuranyl(VI) species could have two possible structures[9] (Figure 9). Regarding species (3,10), both possible structures would imply serious disorder in the U═O and U−O_{eq} bonds of the linear O═U═O group because either the three uranyl(VI) groups are not surrounded by the same number of hydroxide ligands (Figure 9a1) or each uranium atom is linked to

dx.doi.org/10.1021/ic101953q |*Inorg. Chem.* 2011, 50, 2811–2823

two single oxygen atoms, one above and one below the uranium triangular plane (Figure 9a2). Both structures would lead to a significant wavenumber drift, a broadening, and/or a splitting of the Raman bands, and the Raman/IR exclusion rule would not be respected anymore. Furthermore, the UV−visible electronic absorption spectra of uranyl(VI) solutions would be characterized by a more dramatic change in the absorption band intensity than the measured spectra. Indeed, the increase of the molar absorption due to oligomerization (and therefore to the structure change) in acidic media was considerable.[28] Both Raman and IR-ATR spectra show a progressive and smooth band shift as $-\log mH^+$ increases. The UV−visible electronic absorption spectra were characterized by a progressive increase and decrease of the absorption intensity as a function of $-\log mH^+$. Therefore, the hydrolysis of the uranyl(VI) ion occurs without a dramatic change in the structure of uranyl(VI) species with respect to species (3,5). It is thus reasonable to assign the two couples of vibrational bands at {815; 916} and {793; 868} cm^{-1} to the trimers (3,8) and (3,11), respectively (Table 1). The corresponding suggested structures derive from the stable (3,5) structure[38] and lead to smaller disorder (Figure 9b,c).

Because in an acidic medium the same species were found in H_2O and in D_2O, it is suggested that it was also true in basic solutions. The uranyl(VI) hydrolysis should be the same in both media. Moreover, the same wavenumbers were expected for scattering bands of species with the same structure. Samples in D_2O were difficult to obtain; the $-\log mD^+$ range explored was reduced to 12.72−13.84. Bands for species (3,8) were not observed in the spectra because this species was in negligible quantity at $-\log mD^+ \geq 12.8$, and the spectra did not show any scattering band near 815 cm^{-1}. The BPSS estimated band at 790 cm^{-1} was very close to that estimated in the Raman spectra in H_2O. As in H_2O similar solutions, its concentration tended to decrease with an increase of $-\log mD^+$. This band is easily assigned to species (3,11). The estimated band at 777 cm^{-1} that increased with the $-\log mD^+$ value is therefore mainly assigned to species (1,4). The wavenumber shifts with respect to the spectra recorded in H_2O, and the asymmetry of the band could be due to a weak contribution of a band assigned to species (1,5) at lower wavenumber and not resolved by the BPSS process. Whereas no band profile was imposed in the BPSS calculations, a symmetrical Gaussian band shape was used in the decomposition process, leading to the determination of an additional band. Two suggestions can therefore be made: (1) the nonsymmetrical band obtained from BPSS calculations can be the result of an exchange process in the complex species; (2) an additional band is necessary to fit the Raman profile and, as a consequence, an additional species. Three species may therefore be determined at 796, 784, and 767 cm^{-1} in D_2O. They were assigned to species (3,11), (1,4), and (1,5), respectively.

As for the Raman spectra, the two bands at 854 and 843 cm^{-1} were estimated by BPSS from the IR-ATR spectra [Figure 5(II)]. As in H_2O solutions, the difference spectra in Figure 4(II) show three bands. They were located at 868, 854, and 834 cm^{-1}. As indicated in the Results section, three bands were also expected from the BPSS calculation. However, the program did not converge with three components. This was probably due to a too much soft evolution of the IR profile and to very high fwhh's of the absorption bands. By a comparison with the assignments made for samples in H_2O solutions, the above three bands were assigned to species (3,11), (1,4) and (1,5), respectively. At last, IR band wavenumbers of uranyl complex species have lower values in spectra recorded in D_2O solutions with respect to those recorded in H_2O solutions. Again, this was probably due to the characteristics of the asymmetric stretching mode involved. Indeed, the uranium atom moves with the heavier OD and D_2O ligands, leading to a lower wavenumber in D_2O for species with identical numbers of ligands. This assumption was supported by attenuation of the wavenumber difference with a lowering of the number of water molecules in the complex species.

CONCLUSIONS

A combination of three optical spectroscopies completed with data processing of the vibrational spectra in basic solutions allowed characterization of the dominant hydrolyzed uranyl(VI) species in the presence of noncomplexing electrolytes, over a wide and thorough $-\log mH(D)^+$ range. Notably, we have successfully applied a statistical curve resolution method (BPSS) to noisy spectra. In basic solutions, spectral data of this work represent a link between potentiometric data at low uranyl(VI) concentration (<0.005 M) and $-\log mH^+ \leq 12$ and EXAFS and NMR measurements at higher uranyl(VI) concentration (0.05−0.1 M) and in strongly basic solutions, $-\log mH^+ > 14$. The use of the TEAOH organic base prevented precipitation of uranate salts without spectroscopic interference. Raman and IR-ATR bands were tentatively assigned to two trimers and three monomers of uranyl(VI) hydroxides. In both H_2O and D_2O solutions, all of the species found were the same, and each species had only one symmetric and one antisymmetric stretching mode. Therefore, this work, which analyzed spectroscopic data with statistical methods, is of interest to the actinide community. Indeed, it allows identification of trimeric species for pH values below 13 at uranium concentrations above 10^{-4} M. The existence of a new monomer with the highest number of OH^- ligands, $UO_2(OH)_6^{4-}$, was also suggested for the first time in the strongest basic solutions. The wavenumbers of the stretching mode decrease as the number of $OH(D)^-$ ligands increases. However, the band characteristics of the uranyl stretching mode changed in D_2O compared to those in H_2O in the IR-ATR spectra but not in the Raman spectra. Absorption wavenumbers and fwhh's have lower values, and the "effect" decreased with an increase of the number of OD ligands. They were assigned to mechanical coupling and molecular exchanges in the different uranyl complexes.

ASSOCIATED CONTENT

Supporting Information. Raman and IR-ATR spectra of TEAOH and TMAOH in the presence or not of uranyl(VI) in H_2O and those used in the BPSS statistical approach and a list of the solutions analyzed [total uranyl(VI) concentration and $-\log mH(D)^+$]. This material is available free of charge via the Internet at http://pubs.acs.org.

AUTHOR INFORMATION

Corresponding Author

*E-mail: fabienne.quiles@lcpme.cnrs-nancy.fr. Fax: +33 (0) 383 27 54 44.

Present Addresses

[†]G2R, CNRS, Nancy-Université, Boulevard des Aiguillettes, BP 239, F-54506 Vandoeuvre-lès-Nancy, France.

[‡]IMN, 2 rue de la Houssinière, BP 32229, F-44322 Nantes Cedex 3, France.

■ ACKNOWLEDGMENT

The authors thank Dr. D. A. Palmer (Oak Ridge National Laboratory, Oak Ridge, TN) for fruitful discussions and Dr. C. Ewels for rereading the text. J. Cortot and J. Grausem (LCPME-UMR CNRS 7564, Villers-lès-Nancy, France) are acknowledged for their technical assistance.

■ REFERENCES

(1) Maya, L.; Begun, G. M. *J. Inorg. Nucl. Chem.* **1981**, *43* (11), 2827–2832.
(2) Toth, L. M.; Begun, G. M. *J. Phys. Chem.* **1981**, *85*, 547–549.
(3) Nguyen-Trung, C.; Begun, G. M.; Palmer, D. A. *Inorg. Chem.* **1992**, *31*, 5280–5287.
(4) Palmer, D. A.; Nguyen-Trung, C. *J. Solution Chem.* **1995**, *24* (12), 1281–1291.
(5) Clark, D. L.; Conradson, S. D.; Donohoe, R. J.; Keogh, D. W.; Morris, D. E.; Palmer, P. D.; Rogers, R. D.; Tait, C. D. *Inorg. Chem.* **1999**, *38*, 1456–1466.
(6) Wahlgren, U.; Moll, H.; Grenthe, I.; Schimmelpfennig, B.; Maron, L.; Vallet, V.; Gropen, O. *J. Phys. Chem. A* **1999**, *103* (41), 8257–8264.
(7) Moll, H.; Reich, T.; Szabó, Z. *Radiochim. Acta* **2000**, *88*, 411–415.
(8) Moulin, C.; Charron, N.; Plancque, G.; Virelizier, H. *Appl. Spectrosc.* **2000**, *54* (6), 843–848.
(9) Nguyen-Trung, C.; Palmer, D. A.; Begun, G. M.; Peiffert, C.; Mesmer, R. E. *J. Solution Chem.* **2000**, *29* (2), 101–129.
(10) Quilès, F.; Burneau, A. *Vib. Spectrosc.* **2000**, *23* (2), 231–241.
(11) Brown, P. L. *Radiochim. Acta* **2002**, *90* (9−11), 589–593.
(12) Kimura, T.; Nagaishi, R.; Ozaki, T.; Arisaka, M.; Yoshida, Z. *J. Nucl. Sci. Technol.* **2002**, No. Suppl. 3, 233–239.
(13) Redkin, A. F.; Wood, S. A. *Geochem. Int.* **2007**, *45* (11), 1111–1123.
(14) In this paper, the term $-\log mH^+$ is used instead of the conventional pH. Indeed, many experiments have been carried out at extreme conditions of basicity, pH > 13, where pH cannot be measured with a pH meter.
(15) Guillaumont, R.; Fanghänel, T.; Fuger, J.; Grenthe, I.; Neck, V.; Palmer, D. A.; Rand, M. H. *Update on the chemical thermodynamics of uranium, neptunium, plutonium, americium and technicium*; Elsevier: Amsterdam, The Netherlands, 2003; Vol. 5.
(16) Müller, K.; Foerstendorf, H.; Tsushima, S.; Brendler, V.; Bernhard, G. *J. Phys. Chem. A* **2009**, *113*, 6626–6632.
(17) Grenthe, I.; Fuger, J.; Konings, R. J. M.; Lemire, R. J.; Muller, A. B.; Nguyen-Trung, C.; Wanner, H. *Chemical Thermodynamics of Uranium*; North-Holland/Elsevier Sci. Pub. Co. Inc.: Amsterdam, The Netherlands, 1992.
(18) Müller, K.; Brendler, V.; Foerstendorf, H. *Inorg. Chem.* **2008**, *47* (21), 10127–10134.
(19) Gal, M.; Goggin, P. L.; Mink, J. *Spectrochim. Acta* **1992**, *48A* (1), 121–132.
(20) Quilès, F.; Burneau, A. *Vib. Spectrosc.* **1998**, *18* (1), 61–75.
(21) Pasilis, S. P.; Pemberton, J. E. *Inorg. Chem.* **2003**, *42* (21), 6793–6800.
(22) Quach, D. L.; Wai, C. M.; Pasilis, S. P. *Inorg. Chem.* **2010**, *49* (18), 8568–8572.
(23) Bullock, J. I. *J. Chem. Soc. A* **1969**, *5*, 781–784.
(24) Shamov, G. A.; Schreckenbach, G. *J. Am. Chem. Soc.* **2008**, *130*, 13735–13744.
(25) Tsushima, S.; Reich, T. *Chem. Phys. Lett.* **2001**, *347*, 127–132.
(26) Bell, J. T.; Biggers, R. E. *J. Mol. Spectrosc.* **1967**, *22* (3), 262–271.
(27) Musikas, C. *Radiochem. Radioanal. Lett.* **1972**, *11* (5), 307–316.
(28) Meinrath, G. *Radiochim. Acta* **1997**, *77*, 221–234.
(29) Dai, S.; Burleigh, M. C.; Simonson, J. M.; Mesmer, R. E.; Xue, Z. I. *Radiochim. Acta* **1998**, *81*, 195–199.
(30) Moussaoui, S.; Brie, D.; Carteret, C.; Mohammad-Djafari, A. *Application of Bayesian non-negative source separation to mixture analysis in spectroscopy*; American Institute of Physics: College Park, MD, 2004; pp 237−244.
(31) Moussaoui, S.; Carteret, C.; Brie, D.; Mohammad-Djafari, A. *Chemom. Intell. Lab. Syst.* **2006**, *81* (2), 137–148.
(32) Moussaoui, S.; Brie, D.; Mohammad-Djafari, A.; Carteret, C. *IEEE Trans. Acoust., Speech, Signal Process.* **2006**, *54* (11), 4133–4145.
(33) Dobigeon, N.; Moussaoui, S.; Tourneret, J. Y.; Carteret, C. *Signal Process.* **2009**, *89*, 2657–2669.
(34) Carteret, C.; Dandeu, A.; Moussaoui, S.; Muhr, H.; Humbert, B.; Plasari, E. *Cryst. Growth Des.* **2009**, *9* (2), 807–812.
(35) Cordfunke, E. H. P.; Ouweltjes, W.; Prins, G. *J. Chem. Thermodyn.* **2004**, *7* (12), 1137–1142.
(36) Glasoe, P. K.; Long, F. A. *J. Phys. Chem.* **1960**, *64*, 188–190.
(37) Aberg, M. *Acta Chem. Scand.* **1969**, *23*, 791–810.
(38) Aberg, M. *Acta Chem. Scand.* **1978**, *A32* (2), 101–107.
(39) Koglin, E.; Shenk, H. J.; Schwochau, K. *Spectrochim. Acta* **1979**, *35A*, 641–647.
(40) Anderson, A.; Chieh, C.; Irish, D. E.; Tong, J. P. K. *Can. J. Chem.* **1980**, *58* (16), 1651–1658.